5.11 Nanoimprint Lithography and Its Application in Tissue Engineering and Biosensing

K Li, K Morton, and T Veres, Industrial Materials Institute, Boucherville, QC, Canada
B Cui, Waterloo Institute for Nanotechnology (WIN), Waterloo, ON, Canada

5.11.1 Introduction 126
5.11.2 Biosensing Applications of NIL 127
5.11.2.1 NIL Nanostructures used as SPR Devices 127
5.11.2.1.1 Propagating SPR and Localized SPR 127
5.11.2.1.2 Extraordinary optical transmission biosensor 128
5.11.2.1.3 SPR/LSPR biosensor fabricated by using NIL 129
5.11.2.1.4 SERS biosensor 129
5.11.2.2 Nonplasmonic Optical Biosensors 131
5.11.2.3 Electrical and Electrochemical Biosensors 132
5.11.2.4 NIL Application in NEMS-Based Biosensor 133
5.11.2.5 Fabrication of Micro-Nanofluidics Using NIL 134
5.11.2.6 Summary 135
5.11.3 Application of NIL in Tissue Engineering 135
5.11.3.1 Introduction 135
5.11.3.2 Different Feature Sizes and Cues That Cell Reacts to 135
5.11.3.3 Examples of Application of NIL in Tissue Engineering 135
5.11.4 Appendix: Additional References 137
5.11.4.1 Additional References for Biosensors 137
5.11.4.2 Additional References in SERS and Optofluidic Biosensor 138
5.11.4.3 Additional References in the Application of NIL for the Fabrication of FET and Nanofluidics, and for Tissue Engineering 138
References 138
Relevant Websites 139

Glossary

contact guidance The phenomenon that anisotropic topographic features induce cells to align along the direction of the anisotropy.

extraordinary optical transmission Greatly enhanced transmission of light through a periodic subwavelength hole array in an otherwise opaque metallic film, which is due to light coupling by surface plasmon resonance.

nano-electromechanical system (NEMS) Miniaturization into the nanoscale of so-called micro-electromechanical system (MEMS). Like MEMS, it typically integrates electronics with mechanical actuators, pumps, or motors, and may thereby form physical, biological, and chemical sensors.

nanofluidics Study of the behavior, manipulation, and control of fluids (that may contain nanoparticles or biomolecules) confined to nanoscale cavities or channels. Fluids so-confined exhibit physical behaviors not observed in larger structures.

nanoimprint lithography Mechanical molding or embossing process where the surface pattern on a mold is duplicated into a material called resist. It offers high resolution superior to that of electron beam lithography, and high throughput comparable to that of photolithography.

Raman scattering Inelastic scattering of light with the lattice in a solid or a molecule, where the photon either gains or loses energy by absorbing or exciting a phonon. As a result, the frequency of the photon is shifted after scattering.

surface-enhanced Raman scattering (or spectroscopy) Enormous enhancement (up to 10^{12}) of Raman scattering when a molecule is adsorbed on a metallic nanostructure or a nanostructured surface. The enhancement is mainly due to the localized surface plasmon resonance on the nanostructure.

surface plasmon When subject to a time-varying electric or electromagnetic field, free electrons will oscillate collectively and coherently near the surface of a conductor or the interface of a conductor and a dielectric material. Such an oscillation is quantized as surface plasmons. For most metals, the resonance frequency lies in the ultraviolet to near-infrared range.

5.11.1 Introduction

Nanoimprint lithography (NIL) [1, 2] is a next generation solution for low-cost, wafer-scale nanopatterning with demonstrated resolution down to 2 nm. It is based on mechanical deformation of a material called resist. Besides ultrahigh resolution, it also offers high throughput and low cost, and is considered as the most promising nanolithography technique for applications other than integrated circuit. In a standard NIL process, an imprint mold or master is used to physically pattern a thin polymer layer prespun on a substrate such as a silicon or glass wafer; and the polymer layer can itself be a functional material or act as an etching mask or liftoff layer for transferring the imprinted pattern into the underlying substrate or another material. Due to the high fidelity of the imprint process, all features, including defects and surface roughness, are replicated precisely and that makes initial mold quality a critical issue. Master molds made by electron beam lithography can be expensive, especially over large areas; however, the possibility of massive replication by NIL significantly alleviates this initial capital investment. Cost reductions can also be gained by using alternative mastering technologies such as interference lithography that can produce periodic structures with period down to 50 nm over wafer-scale areas.

The choice of imprint resist and the way it is set or cured before the master mold is released divide the NIL technique into two broad classes: thermal NIL and ultraviolet (UV)-NIL which that are both used regularly. In thermal NIL (also called hot-embossing NIL), (**Figure 1**(**a**)), a thermoplastic polymer is embossed by the master above the polymer's glass transition temperature, allowing the molten polymer to flow and fill the mold pattern. The applied pressure is maintained during cooling to below the glass transition temperature, thus producing a solid replica. UV-NIL (**Figure 1**(**b**)) uses UV-curable resist which allows for room-temperature processing in applications where the underlying substrate is sensitive to embossing temperatures and/or temperature cycling. Imprint pressure can also be significantly lowered or even reduced to zero by using liquid resist formulations that have low viscosity and low surface energy before cross-linking. In UV-NIL, the molds are typically transparent to UV and visible light, enabling alignment of mold patterns to existing substrate features. Because the entire substrate–mold sandwich is not heated as a unit, UV-NIL is amenable to step and flash where a small die is imprinted in series across a larger wafer, much like a conventional photolithography stepper.

Besides thermal and UV-NIL, other variations of NIL have been developed such as reverse NIL and replication molding (**Figure 1**(**c**)) where the liquid prepolymer is cast onto a mold without external pressure, and then cured in place by either thermal or UV cross-linking. The cured material can then be peeled off, transferred to a secondary substrate or even onto a previously patterned layer to build up a three-dimensional (3D) nanoscaffold. Casted structures can be used directly as a functional substrate or as a new negative mold for imprinting, thus greatly increasing the lifetime of the original master mold. Furthermore, variations within each class allow for flexibility in downstream processing. For example, multilayer resist structures are frequently used in both thermal and UV-NIL in order to facilitate pattern transfer to the substrate.

As already mentioned, the imprinted polymer layer can be a functional material or (if the layer is thick enough for handling) even the substrate itself, depending on the final application. This type of processing is particularly useful for plastic biosensing devices where the packaged sensors may be widely distributed or even disposable so that low per-unit fabrication cost becomes important. In such a situation, further pattern transfer is unnecessary; instead, subsequent surface modification steps or surface coatings provide functionality. It is also possible to imprint quasi-3D structures directly or imprint continuously in a roll-to-roll fashion.

In the field of biosensor technology, NIL's core competency is cost-efficient patterning at relevant length scales such as the wavelength of an interrogating light source for plasmonic sensing. This cost-efficient and high-throughput technique opens new avenues for nanobiosensors that often require many samples in order to probe the variability in biological systems. In the field of tissue engineering, NIL (hot embossing) provides a low-cost and high-throughput route for the fabrication of micro- and

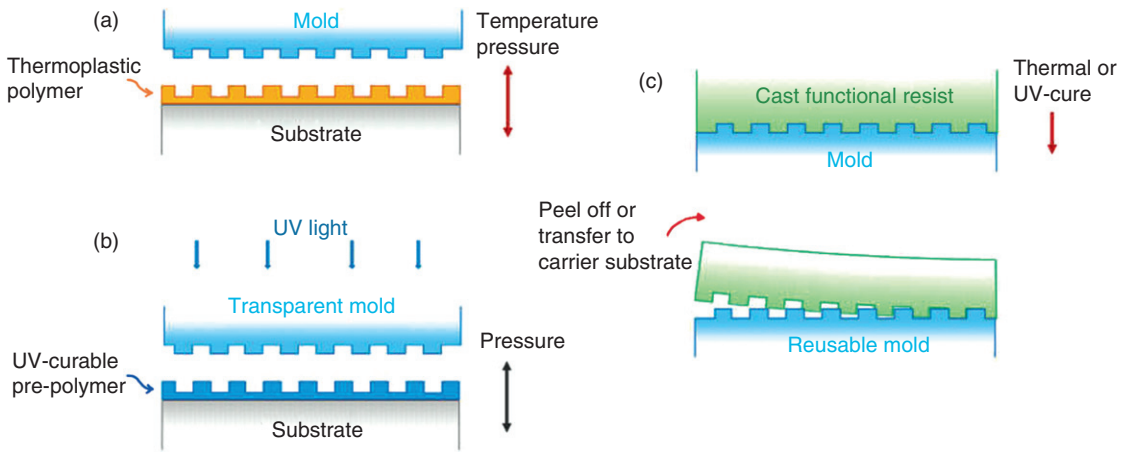

Figure 1 Schematic of nanoimprint lithography (NIL). (a) thermal NIL; (b) UV-NIL; and (c) replication molding.

nanostructured plastic substrate for contact guidance of cell growth. Unlike photolithography that can also pattern polymers by lithography followed by pattern transfer via etching, hot embossing creates a pattern inside a polymer within a single step. It is suitable for patterning a broad range of thermoplastic polymers including those that are biodegradable and biocompatible. In addition, hot embossing is a dry process, which is essential for patterning polymers susceptible to degradation by solvents, water, or other chemicals, whereas many polymer materials such as some biodegradable polymers are not compatible with the solvents and/or the developers used.

5.11.2 Biosensing Applications of NIL

Biosensors based on nanotechnology are rapidly developing and are becoming widespread in the biomedical field and analytical chemistry. In some senses, biosensors usually refer to the nano-biosensors. The advantages of nanotechnological approaches to biosensor development have been addressed in a recent review article by Khanna [3]. The recent progress in the tiny medicine utilizing nanomaterial-based biosensors has been reviewed by Yun *et al.* [4]. According to the detection mechanism, they divided the nano-biosensors into four groups: optical method, electrochemical method, mass detection method, and acoustic method. Many optical biosensors are based on the phenomenon of surface plasmon resonance (SPR) and evanescent wave technique. Other optical biosensors are mainly based on changes in absorbance or fluorescence of an appropriate indicator compound. Electrochemical biosensors are normally based on enzymatic catalysis of a reaction that produces or consumes electrons (such enzymes are rightly called redox enzymes). Mass biosensors are mainly based on the piezoelectric characteristics of some crystals that detect the change of the oscillation frequency of the crystal upon mass change at its surface due to receptor–target binding. The cantilever-based biosensors are good examples of these mass and acoustic-based biosensors. The basic working principles and the types of sensor format, the fabrication and the reported applications in chemical and biological analysis, and trends in microcantilevers fabrication have been reviewed in an article titled 'Nanomechanical biosensors: A new sensing tool' by Carrascosa *et al.* [5].

For biomedical applications, these nano-biosensors must be integrated with appropriate packaging techniques, which are usually based on nano- or micro-fluidics. They are facing many challenges such as dependability, cost, measurement precision, speed, and sample throughput. By introducing advanced materials and advanced device fabrication technique, the nanotechnology-based platforms have the potential to meet these requirements [6].

The high-resolution and high-throughput capability of NIL makes it a very useful technique in the fabrication of nano-biosensors that require precision patterning of large areas with nanoscale structures. The applications of NIL in nano-biosensors are straightforward, and they are involved in all kinds of nano-biosensors that require the fabrication of nanostructures or nanofluidic devices. Some of the NIL applications in biotechnologies have been reviewed by Montelius and Heidari [7]. Basically, it can be classified into two groups: the fabrication of the nanostructures used as the biological active surfaces and the fabrication of micro- and nanofluidics and its lab-on-a-chip (LOC) devices. We will focus on the NIL applications in the fabrication of biosensors, though the recent development of NIL in the fabrication of the micro- and nanofluidic channels for DNA stretching and label-free detection will also be briefly presented. In each subtopic, we will first present the physical mechanism of the related biosensors, followed by giving some examples of the application of NIL in the biosensors involved.

The application of NIL in the fabrication of biosensors includes the following four subcategories: (1) NIL nanostructures used as SPR devices; (2) NIL nanostructures used as nonplasmonic optical biosensors; (3) NIL applications in electrical or electrochemical biosensors; and (4) NIL in nano-electromechanical system (NEMS)-based biosensors. Two types of biosensors, the localized SPR biosensor and the surface-enhanced Raman scattering (SERS) biosensor, are related to the SPR effect.

5.11.2.1 NIL Nanostructures used as SPR Devices

5.11.2.1.1 Propagating SPR and Localized SPR

The interaction between light and metallic nanostructures can lead to interesting charge-density excitations and unique electromagnetic effects, namely the surface plasmons (SPs) and the SPRs. It exists as propagating waves on planar metal films with amplitude that extends further into the dielectric region with decay length on the order of 200 nm, as shown in **Figure 2**(**a**). As the propagation constant of SP at a metal–dielectric interface is larger than the wave number of the light wave in the dielectric, SPs

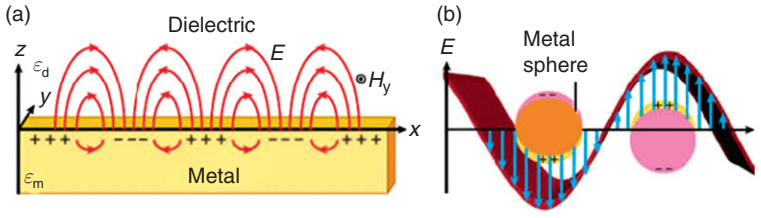

Figure 2 (a) Surface plasmon polaritons at a metal–dielectric interface and (b) localized surface plasmons on a metal nanoparticle excited by free-space light.

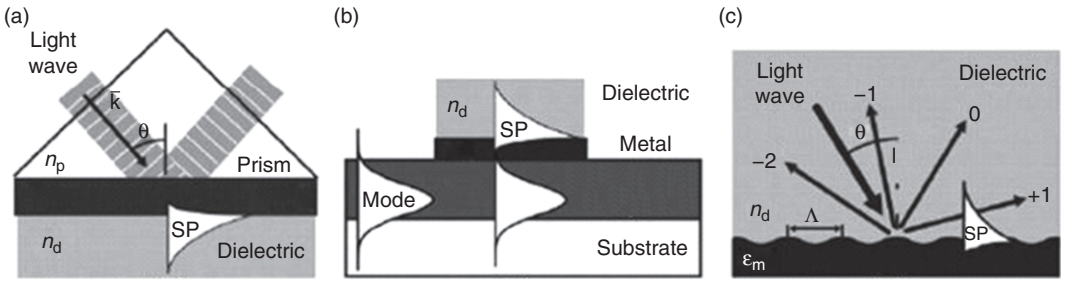

Figure 3 Coupling of light to surface plasmon via (a) prism coupler; (b) waveguide coupler; and (c) grating coupler.

cannot be excited directly by light incident onto a smooth metal surface. The wave vector of light can be increased to match that of the SP by attenuated total reflection or light diffraction. This enhancement and the subsequent coupling between light and SP is performed in a coupling device (coupler). The most common couplers used in SPR sensors include prism coupler, waveguide coupler, and grating coupler, as shown in **Figure 3** [8]. The interaction between the metal surface-confined electromagnetic wave and a molecular surface layer of interest leads to shift in the plasmon resonance condition, which can be observed in the form of shifted peak or valley angle if wavelength is fixed, shifted resonance wavelength, or changes of light intensity if wavelength and detection configuration are fixed. In the first two modes, one measures the reflectivity of light from the metal surface as a function of either angle of incidence (at constant wavelength) or wavelength (at constant angle of incidence). The third method uses light of both constant wavelength and incident angle to interrogate a two-dimensional region of the sample, mapping the reflectivity of the surface as a function of position [9]. Over the last decade, there has been an increasing interest in the SPR effect due to its fundamental and practical significance. From a fundamental point of view, SPRs are of interest to a wide spectrum of scientists for understanding the physical interaction between light and matter at the nanoscale level. Practically, SPRs are being explored for their potential in optical signal processing, magneto-optic data storage, solar cells, plasmonic devices, as well as sensors for detecting various biomolecules.

Light can interact with particles much smaller than the incident wavelength (**Figure 2(b)**). This leads to a plasmon that oscillates locally around the nanoparticle, which offers the potential for developing new types of photonic devices. The localized SPR (LSPR) frequency is highly sensitive to the size, shape, and dielectric environment of the metal particles or structures. Various methods have been developed to produce nanoparticle arrays and nanostructured films. It has been theoretically predicted that dipolar coupling in one-dimensional (1D) and two-dimensional (2D) nanoparticle arrays can produce very narrow plasmon line shapes and exceptional electromagnetic enhancements. The extremely narrow plasmon resonance line shape has been experimentally observed in Au nanodot arrays, Au disk arrays, and silver-coated Au nanorods. Very recently, Svedendahl *et al.* [10] have made a direct experimental comparison for the refractive index-sensing capability between LSPR in Au nanodisks and propagating SPRs on 50-nm-thick Au films. Their results demonstrated that LSPR sensing based on simple transmission or reflection measurement is highly competitive to the traditional SPR sensor. One potential advantage for LSPR biosensor is that biomolecules are concentrated on the nanostructures, leading to a faster response than propagating SPR, although this requires minimal unspecific binding to the dielectric substrate. Other advantages for LSPR include the low bulk refractive index sensitivity, implying that temperature stabilization is less important, and the simple measurement technique needed (straightforward transmission or reflection, as compared to excitation through a prism).

5.11.2.1.2 Extraordinary optical transmission biosensor

The extraordinary optical transmission (EOT) through subwavelength nanohole arrays was first reported by Ebbesen *et al.* [11]. The transmission peak wavelength can be tuned by changing the film material, the hole size, and the array spacing and geometry. SP plays a critical role in the enhanced transmission: light incident on the hole array excites SP on one side of the film, which then tunnels through the holes and/or increases the efficiency of light transmitted through the holes, and the SP emerged at the opposite side of the film scatters from the hole array and is converted into free-space light. Different characteristics of the EOT have been observed in different configurations of the nanohole arrays such as infinite array of nanoholes, finite array of nanoholes, and microscale array of nanoholes. As shown in **Figure 4**, one can tune the properties of the Au infinite subwavelength nanohole array by changing the refractive index of the top surface from air ($n = 1$) to oil with different refractive indces ($n = 1.5–1.7$). The SPR peaks of the infinite Au nanohole arrays red-shifted with increased n, yet the bulk plasmon remained unchanged [12]. Compared to prism-coupled SPR sensor (commercially available for over 10 years for research labs and hospitals), advantages of EOT biosensor include the following: (1) transmission mode operation at normal incidence makes low-cost portable tools possible; (2) the footprint of EOT device, that is, the area covered by the hole array, can be as small as ~5 μm, over one order smaller than that for prism-coupled SPR sensor (~200 μm), thus enabling detection of thousands of targets in the same chip without sacrifice of sensitivity; (3) the intrinsic sensitivity, in terms of resonant wavelength shift/mass of attached biomaterial over device area, is two to three orders higher, again due to its much smaller device area; and (4) the noncontact optical measurement obviates the need for a prism and index-matching fluid, and greatly facilitates high-resolution imaging for highly parallel arrayed measurement.

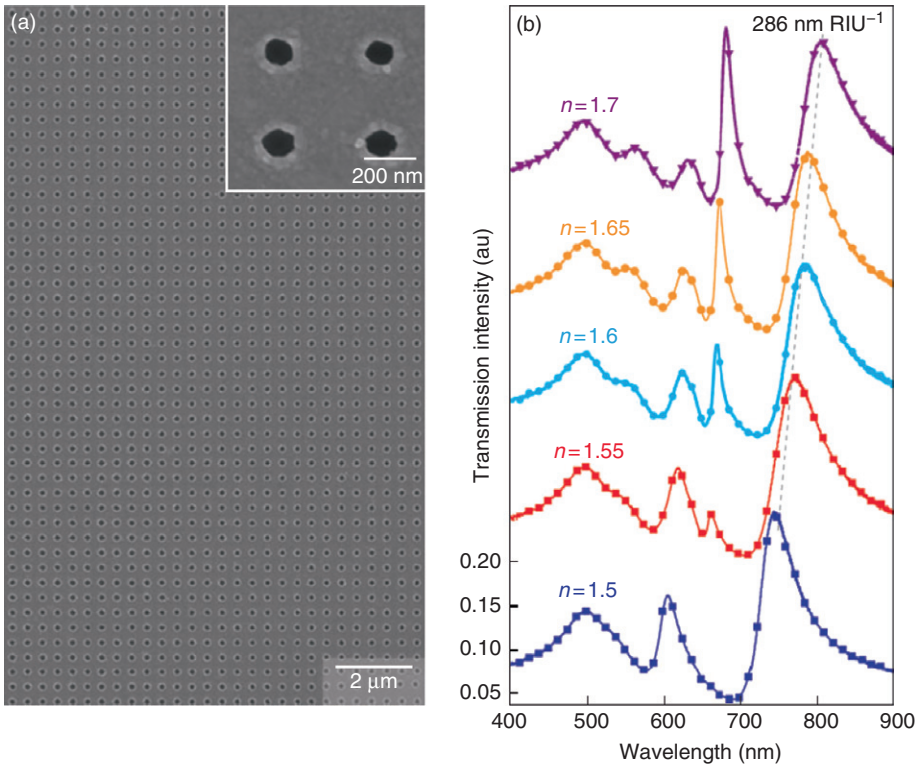

Figure 4 Refractive index sensing using infinite Au nanohole arrays on a glass. (a) Scanning electron microscope (SEM) image of a portion of the infinite Au nanohole array; (b) zero-order transmission in the presence of high-index immersion oils (n = 1.50–1.70). Reproduced with premission from Henzie J, Lee MH, and Odom TW (2007) Multiscale patterning of plasmonic metamaterials *Nature Nanotechnology* 2: 549.

5.11.2.1.3 SPR/LSPR biosensor fabricated by using NIL

NIL provides a general platform for rapid prototyping of nanoparticle arrays with controllable shape, size and, spacing. Boltasseva [13] has reviewed the fabrication of plasmonic components via NIL. Basically, the use of NIL technique for making large-area plasmonic structures can be divided into two categories: those with postprocessing pattern transfer and those without direct imprint into a noble metal film.

Malic *et al.* [14] used NIL to fabricate Au nanogratings that demonstrated 4× SPR signal enhancement compared to unpatterned film in the detection of DNA hybridization process. The enhancement of SPR signal was also observed in an array of micropillars fabricated by NIL [15], which is due to the increase in the surface area of the sensor compared with a planar film. Another advantage is that the pillars themselves can act as waveguides, permitting their use in transmission-coupled LSPR, as recently reported by Jorgenson [16].

Lucas *et al.* [17] used NIL to create uniformly oriented and homogeneous noble metal nanoparticle arrays with well-controlled size, shape, and spacing. For the square Ag array, shown in the inset of **Figure 5**, the extinction spectra clearly show the dependence on the thickness. With increase of the Ag thickness, the LSPR peak is blue-shifted, which suggests that increased damping due to surface scattering may play a non-negligible role. The sensor shows concentration-dependent kinetics of surface adsorption or binding of biomolecules. The ability to monitor antigen–antibody specific reaction has been demonstrated by the reaction between bovine serum albumin (BSA) and anti-BSA immunoglobulin. It demonstrates that NIL can be a very powerful and flexible approach to fabricate large-area noble metal nanostructure arrays and 1D gratings, which have tremendous impact on a number of LSPR applications including tunable filters. As for EOT-based device, an enhancement in transmission has been observed in gold nanohole arrays fabricated by soft UV-NIL [18], which can be used for biochemical sensing.

5.11.2.1.4 SERS biosensor

SERS is another effect where localized SP plays a critical role for the detection of chemical and biological compounds. Since its discovery, SERS has proved to be a sensitive technique able to detect a single molecule. Its chemical specificity and label-free nature have enabled many analytical, biomedical, or environmental applications. The large signal enhancement in SERS mainly originates from the excitation of LSPR in metallic nanostructures. It is important for the LSPR of the enhancing substrate to be properly matched with the Raman excitation and scattering wavelength. The enhancement factor (EF) of the electromagnetic field is rather complex, but approximately

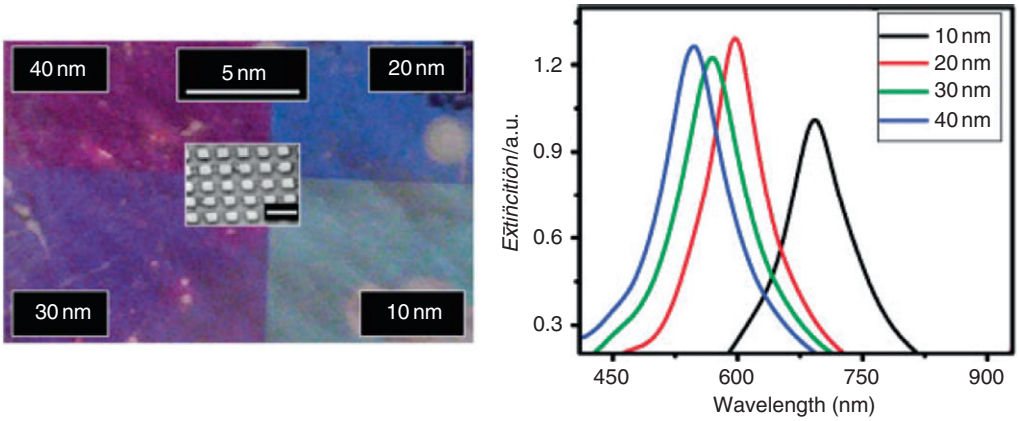

Figure 5 (Left) Photograph of Ag nanostructure arrays that differ in thickness as indicated by labels. The insert shows an SEM image of a square array (scale = 350 nm). (Right) Measured extinction spectra for the four film thicknesses. Reproduced with permission from Lucas BD, Kim, JS, Chin C, and Guo LJ (2008) Nanoimprint lithography based approach for the fabrication of large-area, uniformly-oriented plasmonic arrays. *Advanced Materials* 20: 1129–1134.

$$\mathrm{EF} = \frac{|E_{\mathrm{out}}|^2 |E'_{\mathrm{out}}|^2}{|E_0|^4} = 4g^2 g'^2$$

where the primed symbols refer to the field evaluated at the scattered frequency. If the Stokes shift is small, both g and g' are at approximately the same wavelength, and the EF scales as g^4. In the literature, this is commonly referred to as E^4 enhancement. EF can approach 10^8 in silver nanostructures. The enhancement of the local electromagnetic field has been observed in various nanostructures such as nanodisk array, bowtie nanoantenna, nanoburgers, and nanopins.

By using NIL, we have fabricated various types of metallic nanostructures including Cr nanoring [19], Au and Ag nanocrescents and nanowells [20, 21], Au and Ag nanostars and nanoprisms, nanogratings, and nanopillars [22]. **Figure 6** summarizes some examples of nanostructures fabricated using NIL. SERS enhancement was observed in the Ag nanograting and nanopillars, which was attributed to the LSPR coupling that in turn results from variations in surface nanotopography. In fact, the SERS spectra of naphthalenethiol are enhanced for a given laser wavelength through optimal coupling between the LSPR and the incident laser light, with the LSPR tuned through the control of the surface topography, namely the shape and size of the features, as shown in **Figure 7(a)**. **Figure 7(b)**(A) shows the Raman spectra of human, bovine, and sheep corticotrophin releasing factors (CRFs). **Figure 7(b)**(C, D) show the SERS spectra of the three pure CRFs and their mixtures by using the Ag island film deposited on a nanostructured substrate (**Figure 7(b)**(B)). Both of them show similar vibrational features, but with some characteristic peak differences likely due to subtle conformational variations among the CRFs, which are amplified in SERS. By using the multivariate data analysis method, Alvarez-Puebla *et al.* [23] have shown that peptidic performance enhancers with more than 80% sequence homology could be classified with 100% confidence from simple SERS measurements. They have demonstrated that contaminated samples (mixtures of CRFs) can be readily identified, classified, and even quantified by using the same approach. By using the Au nanowells shown in **Figure 6(d)**, we have also demonstrated that there are two LSPR absorption peaks, with one located in the visible light region and the other in the near-infrared (NIR) region. The advantage of using NIR laser source in SERS detection for biosensing application is to avoid the photochemical

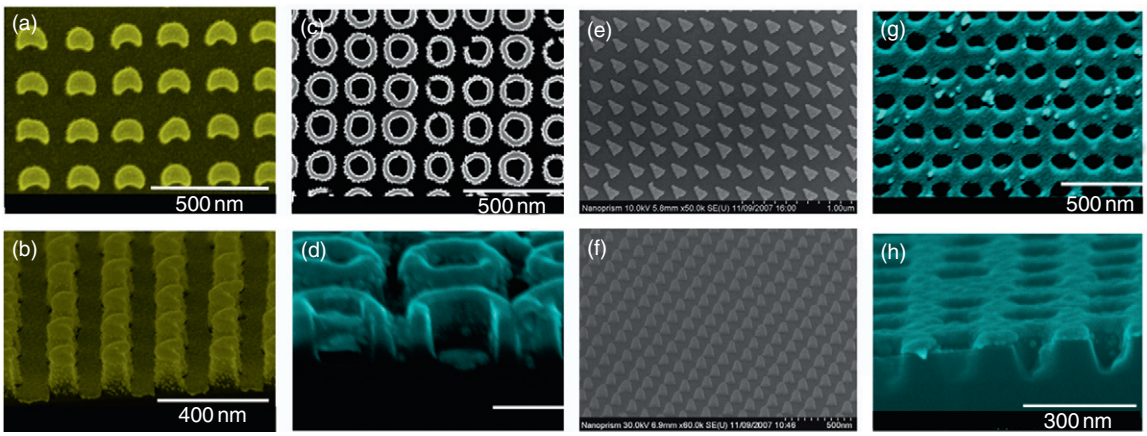

Figure 6 Au nanocrescents (a, b), Ag nanowells (c, d), Ag nanoprisms (e, f), and Ag nanoholes (g, h) fabricated using NIL.

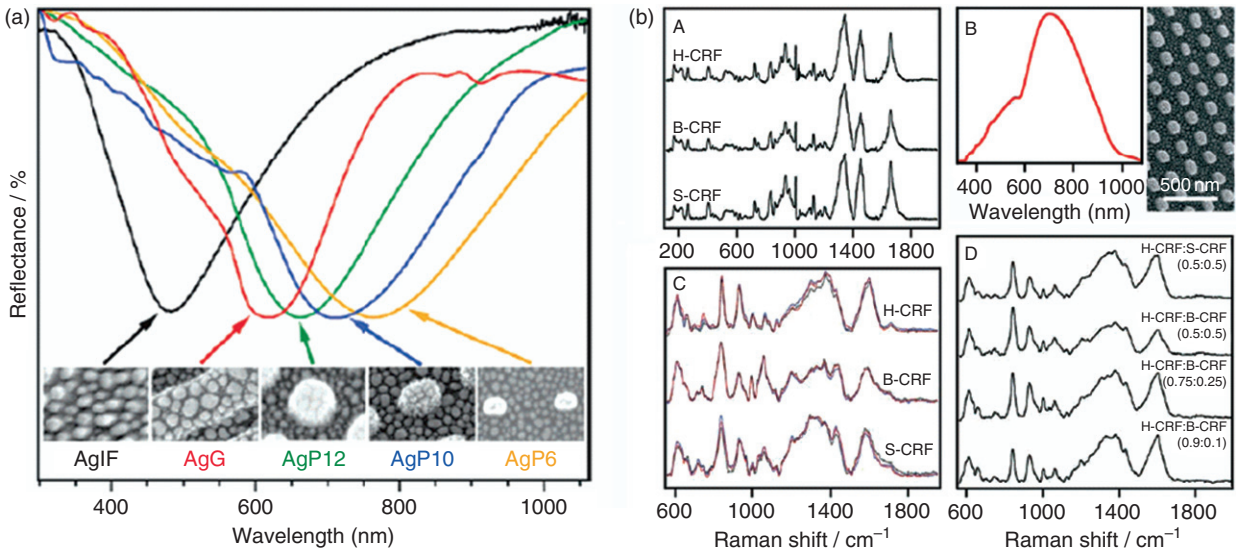

Figure 7 (a) Surface plasmon resonance of Ag-coated flat, grated, and pillared substrates. Insets are 300 × 200 nm^2. (b) Raman and SERS spectra of human, bovine, and sheep corticotrophin releasing factors (CRFs) on nanostructured Ag substrate: (A) Raman spectra of H-CRF, B-CRF, and S-CRF; (B) surface plasmon resonance spectrum and SEM image of the pillared substrate; (C) SERS spectra of pure CRFs; and (D) averaged SERS spectra of CRF mixtures.

reaction on the surface as well as fluorescence from the adsorbed molecules. Such type of nanostructure is the efficient SERS substrate, which can be used to detect label-free DNA molecules [24].

Ag nanoprism array with homogeneous size, shape, and height, and a period of 200 nm and edge length of 100 nm, has been fabricated and tested as an effective substrate for SERS detection [25]. Such an NIL approach can also fabricate nonequilateral nanoprisms and 3D nanopyramid arrays, and it can be readily extended to other metals too. It has been found that the near field is significantly enhanced at the sharp corners of the nanoprism. However, the near field drops greatly with an additional 5 nm Cr usually used as the adhesion layer before deposition of the 20-nm Ag layer. One has to avoid such type of SERS killer in the real biosensor application.

5.11.2.2 Nonplasmonic Optical Biosensors

Photonic waveguide biosensor is an emerging optical technology that has recently been under intensive investigation. It includes planar optical waveguide sensors, directional coupler sensors, Mach–Zehnder interferometric sensors, grating-coupled waveguide sensors, and microresonator sensors [26, 27]. As shown in **Figure 8(a)**, a straight waveguide sensor element consists of a thin Si waveguide wire with dimensions of submicrometer in width and several hundred nanometers in thickness. When light is coupled into this waveguide, it will propagate along the waveguide with negligible loss. The electromagnetic field distribution of the light, or

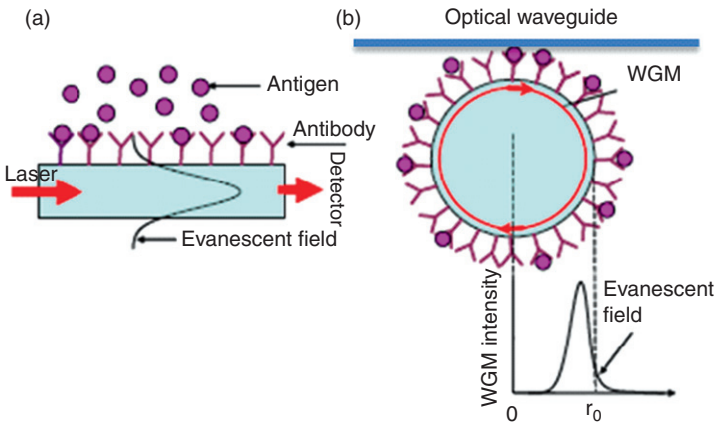

Figure 8 (a) An optical biosensor based on straight waveguide. (b) An optical ring resonator in which the WGM circulates along its surface. Modified from Fan X, White IM, Zhu H, *et al.* (2007) Overview of novel integrated optical ring resonator bio/chemical sensors. *Proceedings of SPIE* 6452: 64520M, with permission of SPIE.

waveguide mode, has an evanescent tail that extends into the surrounding medium for approximately 100 nm and interacts with the biomolecules near the waveguide surface. A small change in refractive index near the waveguide surface when target analyte is captured causes modification in the optical signal (such as its phase) at the output, which acts as the sensing signal. In order to increase the sensitivity in such type of sensor, one has to increase the physical length of the waveguide. However, in an optical microring resonator shown in **Figure 8**(**b**), the light propagates in the form of whispering gallery mode (WGM), which results from the total internal reflection of the light along the curved surface. The WGM is a surface mode, and it circulates along the resonator surface and interacts repeatedly with the analyte on its surface through the WGM evanescent field. The sensitivity of the microring resonator is determined by the effective light–analyte interaction length of a ring resonator sensor, which is characterized by the resonator quality factor, the *Q*-factor. The effective interaction length is given by $L_{\text{eff}} = Q\lambda/2\pi n$, where λ is the wavelength and n is the refractive index of the ring resonator. For a ring resonator with a Q factor of 10^6, $n = 1.45$, and $\lambda = 980$ nm, L_{eff} can be as long as 10 cm; so, a microring resonator sensor can deliver sensing performance even superior to photonic Si-wire waveguide sensor. Densmore *et al.* [28] have fabricated a spiral ring resonator with a total length of 1.3 mm within 130 um spot area. The light–analyte interaction length has been increased both physically and effectively, leading to further increase of the device sensitivity. It has been demonstrated that it can be used to monitor the antibody–antigen reaction in real time. The sensitivity can reach 0.25 pg mm^{-2}, which corresponds to a molecular mass of 0.5 fg. In the design of the microring resonator, the coupling coefficient plays an important role in determining the device characteristics. The coupling coefficient depends exponentially on the gap distance between the ring and the straight waveguide. In order to have sufficient coupling, the gap distance must be less than 200 nm, therefore nanofabrication such as by NIL plays an important role. Chao and Guo [29] have fabricated polystyrene microring resonator using the NIL technique, which produced a Fano-resonant line shape and greatly enhanced the sensitivity of the sensor.

5.11.2.3 Electrical and Electrochemical Biosensors

Electrochemical sensor measures the change in current, voltage, impedance, or conductance resulting from a chemical reaction that either transfers or separates electric charge with reasonable selectivity and sensitivity. Based on their different detection mechanism, they can be classified as amperometric/voltammetric, potentiometric, impedance, and conductometric sensors. All of them rely on the fabrication of an electrode. There are some advantages using the nanoelectrodes in electrochemical biosensors. First, as the current is proportional to the surface area of the electrode, nanoelectrodes will reduce the ohmic drop ($I \times R$) distortion and can be used to detect electrochemical reactions in poorly conducting media. Second, nanoelectrodes can reduce the response time because of reduction of the capacitance that is proportional to the surface area of the electrode. Third, the rate of mass transport to and from the electrode increases as the electrode size decreases, leading to better signal-to-noise ratio and higher sensitivity. **Figure 8** illustrates the difference between the macroelectrode and nanoelectrode and their voltammograms. Planar diffusion is the main mass transport mechanism in the macroelectrode, whereas it is dominated by the radial diffusion mechanism in the nanoelectrodes, corresponding to cyclic voltammogram in the former case and sigmoid curve in the latter [30]. **Figure 9**(**C**) shows an example of the electrochemical biosensor made on multiple-wall carbon-nanotube (CNT) nanoelectrode array. The CNT was grown on a nickel catalyst film of 10–30 nm that was deposited and patterned on a microelectrode pad with a size of few micrometers. A SiO_2 film was

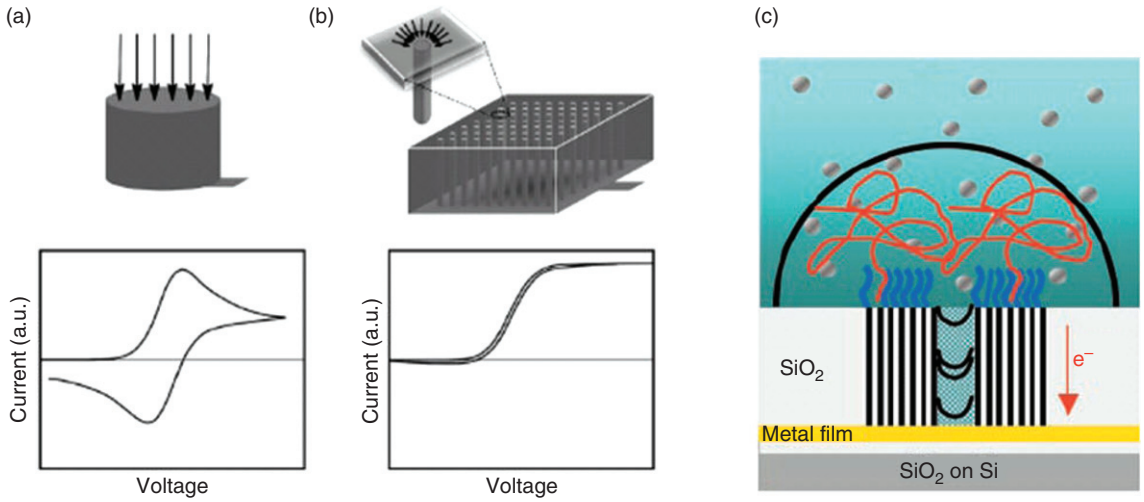

Figure 9 (a) Macroscopic electrode with planar diffusion and its corresponding cyclic voltammogram. (b) One nanoelectrode from the nanoelectrode array with radial diffusion and its steady-state voltammogram when cycling with slow rate. Both measurements were conducted in a redox solution. (c) Multiple-wall carbon-nanotube nanoelectrode used for electrochemical detection of oligonucleotide and PCR amplicon target. (a, b) Reproduced with permission from Wei D, Bailey MJ, Andrew P, and Ryhänen T (2009) Electrochemical biosensors at the nanoscale. *Lab on a Chip* 9: 2123–2131. (c) Reproduced with permission from Koehne JE, Chen H, Cassell AM, *et al.* (2004) Miniaturized multiplex label-free electronic chip for rapid nucleic acid analysis based on carbon nanotube nanoelectrode arrays. *Clinical Chemistry* 50: 1886–1893.

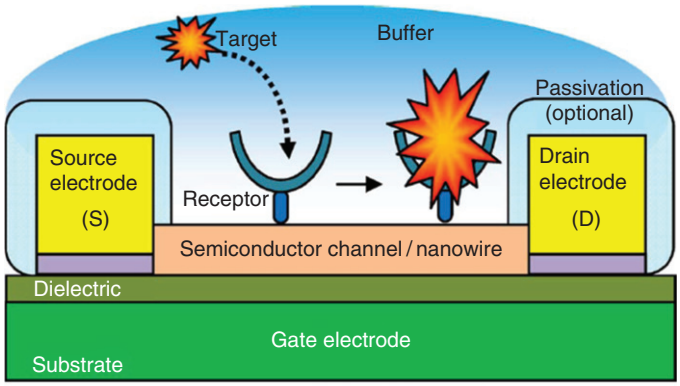

Figure 10 Structure of an FET nanobiosensor. The gate electrode is used to set the conductivity of the semiconductor channel. A receptor molecule attached to the surface of the semiconducting material can specifically recognize and capture a target molecule from a buffer solution, which modifies the conductivity of the semiconductor channel.

deposited by thermal chemical vapor deposition to form a conformal film filling the space between CNTs as well as covering the substrate surface. After chemical mechanical polishing process, only a small number of CNTs that are longer than others are exposed to form a low-density inlaid nanoelectrode array. Koehne *et al.* [31] have successfully employed this device for the detection of the DNA hybridization process. One can apply the NIL technique to fabricate the nickel nanodot array in order to further improve the performance of such type of sensor by placing the CNTs precisely in a periodic array. Sandison *et al.* [32] have fabricated an array of nanoelectrodes with diameter of 250 nm by using NIL method. Tallal *et al.* [33] have demonstrated the ability to reproduce both sub-40-nm nanoelectrodes and micrometric connection pads using single NIL step over a 20-cm wafer, which opens up the possibility to mass-produce electrochemical nanobiosensors.

The field-effect transistor (FET) is a type of transistor that uses an electric field to control the conductivity of a channel between two electrodes in a semiconducting material. As shown in **Figure 10**, the semiconductor channel consists of, for example, a nanowire, and is used as the sensing component of the device [34]. Control of the conductivity is achieved by varying the electric field potential relative to the source and drain electrode at a third electrode, known as the gate. Depending on the configuration and doping of the semiconducting material, the presence of a sufficient positive or negative potential at the gate electrode would either attract charge carriers or repel charge carriers in the conduction channel. This would either fill or empty the depletion region and thus enlarge or shrink the effective electrical dimensions of the conducting channel. An FET can be operated either in a linear mode or in a saturation mode. FET devices are preferred for weak-signal and/or high-impedance applications, hence their widespread use in the growing field of electrochemical biosensing. There are many different types of FET devices that can basically be subdivided into three main groups depending on the type of receptor used for the analyte recognition and on how this signal is generated: (1) enzyme-modified FETs, usually involving the product of a catalytic reaction (e.g., H^+ or H_2O_2 generation or a reaction between an enzyme and its substrate); (2) cell-based FETs, utilizing potential changes that are produced by living biological systems; and (3) immunologically modified FETs and DNA-modified FETs, exploiting surface polarization effects or changes in the dipole moment (e.g., antigen–antibody binding or DNA hybridization). The conversion of an FET into a sensing device normally involves the replacement of the metal gate electrode by a biochemically sensitive surface (e.g., an analyte-selective membrane or an ion-conductive solution), which is brought into contact with the analyte solution. Also present in the analyte solution is a reference electrode, which completes the circuit via the gate-voltage bias. NIL has been used to fabricate metal-oxide semiconductor FETs and organic thin-film transistors. Recently, Gao *et al.* [35] have used NIL to create a silicon nanowire (trapezoidal cross section) with a top width of 22 nm and demonstrated that it could be used as a gas sensor. It indicates that NIL can be used to fabricate a Si nanowires-based BioFET.

5.11.2.4 NIL Application in NEMS-Based Biosensor

Very recently, Ghatnekar-Nilsson *et al.* [36] have investigated a totally new printable approach to manufacturing NEMSs. The device is based on nanoscale high-aspect-ratio tunable grating structures (interdigitated pairs of walls) fabricated using NIL in a photoresist or a plastic material. The structures are fixed along their length at the bottom, in contrast to free cantilevers, as shown in **Figure 11**. A direct current (DC) voltage applied to the metal layer on top of the structures gives rise to an electrostatic force between the walls so that the upper part of the fingers bend toward each other. Adding an alternating current (AC) voltage causes an oscillatory motion, which allows for frequency response measurements in which the resonance frequency is recorded. This property was used in the application of gas sensing. Airborne molecules may be caught on the sensor surface and by adding their mass to the oscillating walls they reduce the resonance frequency. Besides gas sensing, these devices can also be used as biosensor based on mass sensing, electrical switch and filter, and optical device. Due to its nanoscale size and the use of light materials, the device achieves performance in terms of speed, sensitivity, and versatility that challenges or surpasses the limitations of technological achievement to date. On top of this is the potential of simple low-cost fabrication made possible by developments in NIL.

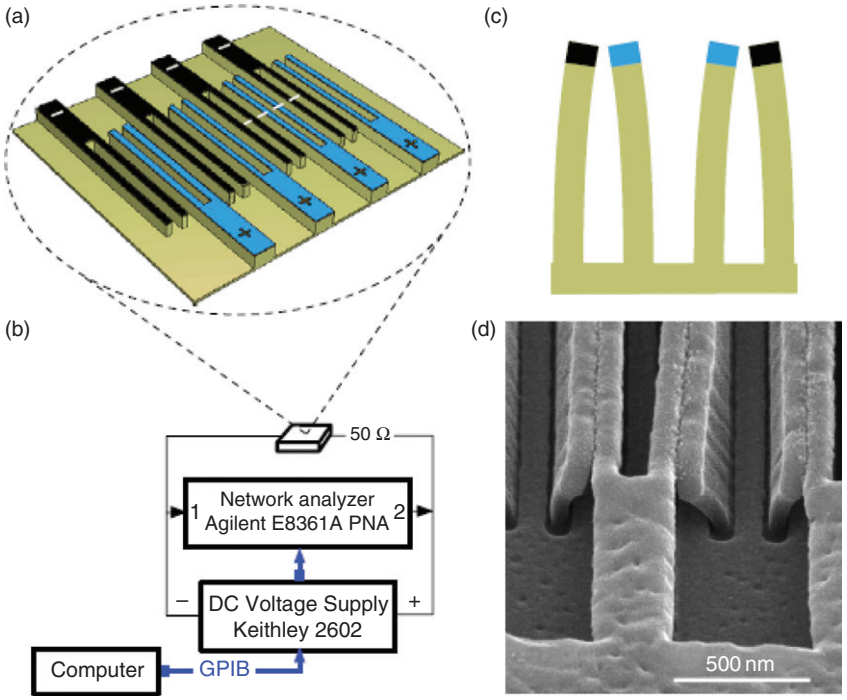

Figure 11 (a) Schematic picture showing the grating with the interdigitated pairs of walls. The top layer of the structures is the same metal, but for clarification it was indicated by the polarities using different colors. (b) An illustration of the measurement setup. (c) The lateral movement of the walls as a DC bias is applied. (d) SEM image shows walls that are intentionally collapsed and short-circuited by applying a high voltage. Reproduced from Ghatnekar-Nilsson S, Karlsson I, Kvennefors A, *et al.* (2009) A new multifunctional platform based on high aspect ratio interdigitated NEMS structures. *Nanotechnology* 20: 175502, with permission of Institute of Physics.

5.11.2.5 Fabrication of Micro-Nanofluidics Using NIL

Nanofluidics has, in recent years, provided new tools for the study of molecular behavior at the single-molecule level, and it is expected to find significant application in biotechnology and medicine. A major application of nanochannels is the analysis of DNA. The confinement of biopolymer such as DNA in nanochannels with dimensions close to the persistence length (length to which a molecule can be laid out in a straight manner) allows for of detecting, analyzing, and separating these biomolecules. Typically, a DNA molecule will form a compact arrangement in its natural state. However, when a DNA molecule flows through a nanochannel with cross many ways section comparable to the persistence length of the molecule, it will be thermodynamically more favorable for the DNA molecule to be in a stretched state, and the degree of stretching is inversely proportional to the channel dimensions. This DNA stretching can lead to important biological applications such as (1) quick mapping of restriction-cut genomic DNA segments; (2) reduction in required DNA sample; (3) localization of transcription factor for protein synthesis to a specific gene or even a specific binding site; (4) parallel analysis; and (5) more sensitive detection with high signal-to-noise ratio.

Another application of nanochannels is in the area of drug delivery. There is presently a need for high-precision nanoengineered device to yield long-term zero-order release of drug for therapeutic applications. Previously, various technologies have been developed to achieve this goal. However, they have a number of shortcomings that are related to (1) degradable polymer implants, which have initial burst effect prior to sustained release of a drug and poor control of release rate for small molecules, and (2) osmotic pumps, which lack the capability of electronic integration for achieving higher level of functionality. Nanochannels fabricated in silicon can allow for the creation of drug delivery that possesses a combination of structural and integrated electronic features that may overcome these challenges.

The most important aspect for fabricating a working nanofluidic system is how to seal the channels. The sealing technique to close up nanotrenches is not as easy as one would first believe. Cao *et al.* [37] have used NIL to create millions of enclosed nanofluidic channels with dimension down to 10 nm. They used the shadowing effect of sputtering where the channels were shrunk and eventually sealed due to the deposition of silicon dioxide onto the sidewall of the trenches. Guo *et al.* [38] have developed a more practical solution to address the issue of enclosing nanochannels. The technique is to simply imprint a channel template into a thin polymer film on a glass substrate without detachment. A very thin polymer layer is used so that the displaced polymer will not be able to completely fill the trenches on the mold. Uniform nanofluidic channels as small as 75 nm × 120 nm were achieved by this method.

Liang *et al.* [39] have extended the fabrication of nanofluidic channels into device level. They used a long nanochannel to stretch a DNA strand into a linear chain. They made a pair of metal wires with a nanogap of 9 nm to measure the electrical conduction perpendicular to the DNA backbone when it passes through the nanogap. When the DNA passes through the gap, it generates a negative electrical pulse signal with duration as long as 388 μs.

5.11.2.6 Summary

In summary, nanostructures fabricated using NIL have been widely used in biosensor applications covering all the four types of plasmonic nanobiosensors, nonplasmonic optical biosensors, electrical and electrochemical biosensors, and mass and acoustic biosensors. They also play an important role in micronanofluidic devices for biological and LOC applications. It would be important to integrate the nanostructured biosensors with micronanofluidics to make an LOC microsystem with sample-in/answer-out capability. NIL fabrication technique based on cheaper and less-fragile polymeric materials will offer an attractive solution to integrate the nanobiosensors with packing technique. Bilenberg *et al*. have made a good attempt to fabricate using NIL a polymer-based LOC microsystem with integrated optics [40]. The LOC contains microfluidic channels and mixers, an absorbance cell, optical waveguides, a microfluidic dye laser, and Fresnel lenses to coup light in and out of the waveguide. Although the absorbance detection was demonstrated in the micrometer-sized structures, the use of NIL makes the technology easily scalable to the nanometer regime. SERS-based optofluidic microsystem is another good example. It involves the integration of nanocolloids or metal nanostructure-embedded substrate with microfluidic systems. The possibility of fabricating by NIL an SERS-active substrate from thermoplastic materials will pave a way for a cheap, disposable platform for label-free detection [41]. It is expected that NIL will be more and more involved in the fabrication of integrated micrototal analysis systems (micro-TASs) for biotechnology applications.

5.11.3 Application of NIL in Tissue Engineering

5.11.3.1 Introduction

While transplant biology has advanced greatly in the past several decades, the supply of donor organs still remains extremely limited. Tissue engineering is a rapidly developing biotechnology domain that offers a promising alternative for wound repair and organ replacement. It is based on the ability of living cells to be assembled *in vitro* as 3D tissues. While the cultivation of 3D functional tissue patches is the ultimate goal, 2D systems may serve as platforms for drug development. In tissue engineering, contact guidance refers to the phenomenon that anisotropic topographic features, such as a grating consisting of grooves and ridges with lateral dimension in the nano-micrometer range, have been shown to induce almost all cell types (except red blood cells) to align and migrate along the direction of the anisotropy.

For the fabrication of substrates for contact guidance of cell growth, most of the initial studies were performed with mineral substrates such as silicon and its oxide or titanium oxide, because these materials are compatible with traditional (Integrated Circuit) IC fabrication techniques. Progress in micromachining processes gradually extended the choice of material to polymers that could be biocompatible and biodegradable. In addition, each micro- or nanostructured substrate must have dimensions of at least several square centimeters in order to perform cellular assays, and tens of to hundreds of samples are necessary for the assays to yield statistically significant results. Therefore, the fabrication technique must offer high throughput and low cost. The choice of fabrication method is naturally NIL based on molding or embossing using known biocompatible polymeric materials.

5.11.3.2 Different Feature Sizes and Cues That Cell Reacts to

In the development of adult animal from the egg, cues are given to dictate proliferating cells' final position and orientation. The cues can be chemical in nature such as adhesion–promoting proteins, or they can be purely physical such as topographical cues. The work of Britland *et al*. [42] is of special interest as they used a chemical cue (laminin) oriented at right angles to a topographic one (grating). When the grooves were 500 nm deep or less, the cells reacted chiefly to the chemical cue. On deeper grooves, the topographic cue overrode the chemical cue and at 5-μm depth the topographic effect oriented about 80% of the cells and the chemical cue 7%.

For topographical cues, the width, depth, and spacing of the grooves all influence the cells' alignment. Contact guidance of cell growth is generally found to be more pronounced on patterns with ridge widths between 1 and 5 μm than wider ones. For narrower (and deep) grooves, cells may bridge from ridge to ridge, so that the cells are effectively reacting only to features of the ridges and not to the recessed grooves. It has been shown that ridges as narrow as 70 nm (pitch 400 nm) could induce human corneal epithelial cells to elongate and align along the features. The depth of the grooves is often more important in determining the degree of alignment than the width, and cells can react to depth well below 100 nm. For instance, macrophage-like cells such as P388D1 cells react to steps as small as 30 nm in height; extensions from some neurons can sense a groove as shallow as 14 nm; and endothelial and fibroblast cells are sensitive to patterns with feature height down to 10 nm. Conversely, the probability that a cell will cross a 10-μm-high step is very low (<10%) and it makes no difference whether the cell has to move up or down the cliff.

5.11.3.3 Examples of Application of NIL in Tissue Engineering

Guillemette and Cui *et al*. patterned polystyrene (a standard tissue culture material) and a thermoplastic elastomer (TPE) by NIL and replication molding with gratings of 4-μm period, and studied not only the effect of surface topography but also cell–extracellular

matrix (ECM) and cell–cell interactions occurring naturally within the cultured tissue [43]. Microstructured TPEs were created by heating it to 170 °C on the mold in air without applying a pressure. TPEs were found as effective as polystyrene in aligning the corneal stromal, dermal, and smooth muscle cells (SMCs), partly because the TPE used in the study consists of 10–12% styrene. It was also observed that the second cell–ECM layer produced is highly organized to a level found only in their physiological tissue counterparts. For human corneal fibroblasts, cell-secreted ECM showed a 60° shift from the previous underlying layer, which is similar in organization to lamellae found in the normal cornea; for SMCs, the angle shift was 30°, which is similar to the native human SMC media arrangement. This aspect of the tissue structure is of critical importance because optical and mechanical properties depend on cell and ECM orientation. For example, the authors found that aligned corneal cells were more transparent (by 11% at 400-nm wavelength) than the control cultured on flat surface; and SMC presented a twofold increase in mechanical strength compared to the control sample.

Matsuzaka *et al*. [44] fabricated polystyrene gratings using replication molding that is one variation of NIL. In the process, the mold was covered by polystyrene casting solution in chloroform, after the evaporation of which polystyrene surface replicas were removed from the mold and used for cell culture. They found that, on the 1-μm and 2-μm-wide groove surfaces, the osteoblast-like cells and their extensions bridged the grooves, whereas, on the wider grooves (5 μm and 10 μm), the extension of the cells adhered to the ridges, into the grooves, as well as the on the groove walls.

Motivated by the natural 3D nanostructure on collagen that has a 400-nm fibrillar width and 70-nm cross-striation, Hu *et al*. fabricated similar 3D nanostructure using two nanoimprint steps, with the second step conducted at temperature lower than the glass transition temperature of the polymer in order to avoid deforming the pattern generated in the first imprint step (see **Figure 12**) [45]. The substrate used for patterning was tissue culture polystyrene surface that is commercially surface-treated and optimized for most adherent cell culture. SMCs were cultured, and were found to align and elongate increasingly as the width of the grating decreased from 10 μm to 350 nm, indicating that nanoscale structures produce more efficient alignment and elongation than microscale patterns for SMCs. In addition, more significant alignment and elongation were observed on grating with deeper grooves.

Johansson *et al*. [46] studied the reaction of neuronal process to grooves and ridges in Poly (methyl methacrylate) PMMA patterned by NIL. The grooves had depths of 300 nm and varying widths of 100–400 nm, and the distance between two adjacent grooves was 100–1600 nm. As shown in **Figure 13**, axons displayed contact guidance on all patterns, and the nerve cells preferred to grow on ridge edges and elevations in the pattern rather than in grooves. In addition, it was found that axonal guidance differs from single-cell guidance as the long axons have a wandering behavior, and even if an axon shows clear contact guidance, it may change to an adjacent ridge.

It would be interesting to study cells' behavior when multiple cues coexist. To this end, Heidi Au *et al*. [47] patterned polystyrene by hot-embossing its pellets, and electroplated Au electrodes such that the grating in polystyrene was orientated either parallel or perpendicular to the electric field direction (see **Figure 14**). Cardiomyocytes were cultured under either topographical or electrical cues, or both. As expected, cardiomyocytes were aligned and elongated forming a well-developed contractile apparatus when either cue existed, and they were significantly more aligned on the gratings parallel to the electric field than those perpendicular. The 1-μm-period grating resulted in a significantly higher elongation than the 4-μm-period grating, and topographical cues were found to be a much stronger determinant of cellular orientation than the electric field stimulation.

Charest *et al*. [48] used NIL to emboss 200-nm-period grating pattern into polycarbonate, and microcontact printing to overlay independent chemical (alkanethiol ink) pattern onto the topography. They found that osteoblast-like cells aligned to and extended along the nanogrooves on a substrate with a uniform chemistry. However, on a substrate with a continuous chemical pattern, such as lanes, the cells aligned to and extended along the chemical pattern rather than the orthogonal nanogrooves.

Besides 1D grating or groove structures, cells' response to 2D pillar or hole structures has also been studied. There are differences in cellular response to a square array of circular holes or pillars, and similar features arranged in a hexagonal array [49]. As expected,

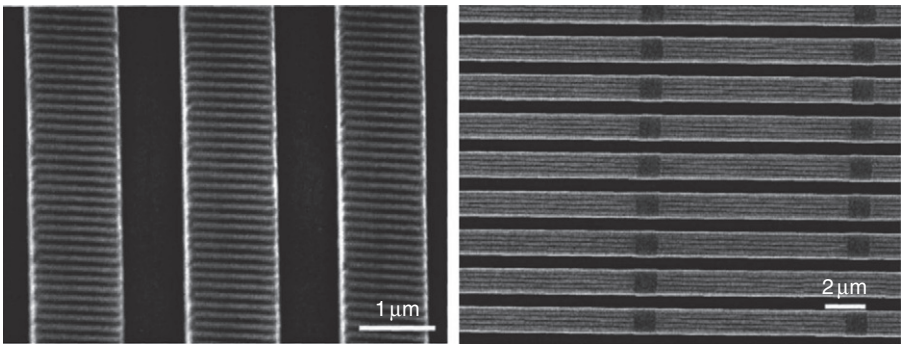

Figure 12 3D polystyrene nanostructures with multiple imprints: 100-nm-wide gratings imprinted on 1-μm half-pitch gratings with (left) perpendicular orientation and (right) parallel orientation. Reproduced with permission from Hu W, Yim EKF, Reano RM, *et al.* (2005) Effects of nanoimprinted patterns in tissue-culture polystyrene on cell behavior. *Journal of Vacuum Science and Technology B* 23(6): 2984–2989. Copyright (2005), American Vacuum Society.

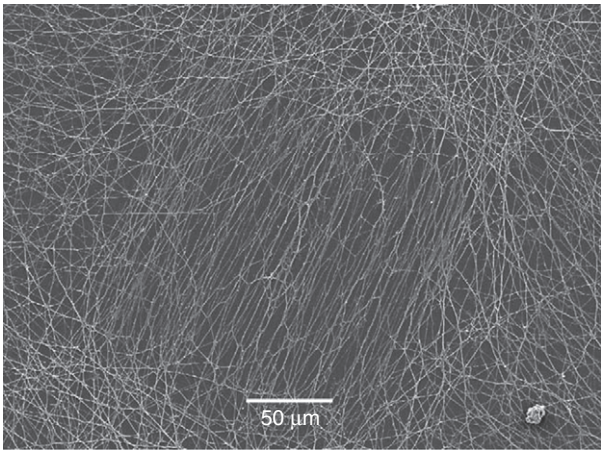

Figure 13 SEM image of axons on an inverted nanoimprinted pattern (200-nm-wide ridges and 1-μm pitch). The inverted pattern shows good macroscopic guidance, even though some axons can be seen to change ridge. The pattern is within a square with side-length of 200 μm that can easily be detected by the aligned axons. Reproduced from Johansson F, Carlberg P, Danielsen N, *et al.* (2006) Axonal outgrowth on nano-imprinted patterns. *Biomaterials* 27: 1251–1258, with permission from Elsevier.

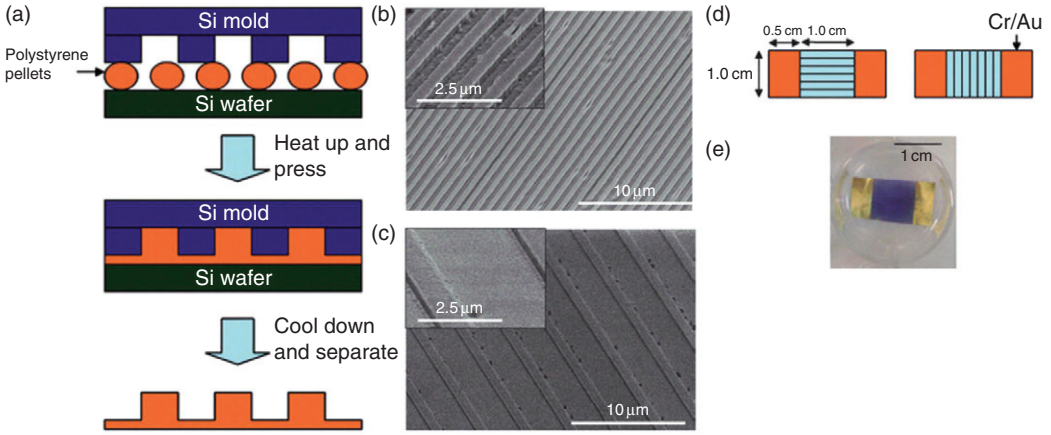

Figure 14 Microgrooved surfaces prepared by hot embossing of polystyrene. (a) Schematics of hot-embossing process. SEM image of the microgrooved surface with (b) 1-μm period, 0.5-μm groove width, 400-nm groove height, and (c) 4-μm period, 3-μm groove width, and 400-nm groove height. (d) Schematics of the orientation of grooves with respect to the electrodes. (e) Photomicrograph of a cell culture chip with cardiomyocytes between electrodes (blue) visualized by Giemsa staining. Reproduced with permssion from Heidi Au HT, Cui B, Chu ZE, *et al.* (2009) Cell culture chips for simultaneous application of topographical and electrical cues enhance phenotype of cardiomyocytes. *Lab on a Chip* 9: 564–575.

cell would not elongate and align in a symmetric 2D array; instead, its adhesion to the substrate is either increased or decreased. For example, using NIL polystyrene substrate was patterned with 300-nm period and 60-nm-diameter 2D square pillar array, and it was found that adhesion of tendon cells to the nanostructured surface was greatly reduced [50]. The cells were seen first approaching and then retreating from the nanostructured surface. As there are many circumstances in which it is desirable to make a surface nonadhesive, the lack of adhesion to nanostructured surface is potentially of great importance in cell engineering.

In summary, due to its high throughput and low cost, along with its capability of patterning directly plastic substrates interesting to tissue engineering, NIL would find great applications in tissue engineering.

5.11.4 Appendix: Additional References

5.11.4.1 Additional References for Biosensors

The recent progress and research in nanosensors have been reviewed by Bogue [51, 52]

Sensors based on surface plasmon have been reviewed by Stewarte *et al.* [53].

The advances in the exploitation of localized surface plasmons resonance (LSPR) in nanobiosensors have been reviewed by Hutter *et al.* [54].

One can also find a review article about the recent progress in LSPR-based nanobiosensors by Sepúlevda *et al.* [55]. For general information about the electrochemical nanobiosensors and their applications for genomic and proteomic analysis as well as the state of art development and its industrial outlook, one can refer to the review articles [56–58].

5.11.4.2 Additional References in SERS and Optofluidic Biosensor

The enhancement of the local EF field has been observed in various types of nanostructures including Au nanodisc arrays [59], bowtie nanoantennas [60], nanoburgers [61], and nanopins [62] .

There are several recent review articles about the fundamental mechanism of SERS and its biochemical and biomedical applications [63–68].

Optofluidic biosensors are good examples of the integration of the optical nanobiosensors with nanomicrofluidics devices [69, 70].

5.11.4.3 Additional References in the Application of NIL for the Fabrication of FET and Nanofluidics, and for Tissue Engineering

[71–79].

References

[1] Chou SY, Krauss PR, and Renstrom PJ (1996) Imprint lithography with 25-nanometer resolution. *Science* 272: 85–87.
[2] Schift H (2008) Nanoimprint lithography: An old story in modern times? A review. *Journal of Vacuum Science and Technology B* 26(2): 458–480.
[3] Khanna VK (2008) New-generation nano-engineered biosensors, enabling nanotechnologies and nanomaterials. *Sensor Review* 28: 39–45.
[4] Yun YH, Eteshola E, Bhattacharya A, *et al.* (2009) Tiny medicine: Nanomaterial-based Biosensors. *Sensors* 9: 9275–9299.
[5] Carrascosa LG, Moreno M, Álvarez M, and Lechuga LM (2006) Nanomechanical biosensors: A new sensing tool. *Trends in Analytical Chemistry* 25: 196–206.
[6] Kim J, Junkin M, Kim DH, *et al.* (2009) Applications, techniques, and microfluidic interfacing for nanoscale biosensing. *Microfluidics and Nanofluidics* 7: 149–167.
[7] Montelius L and Heidari B (2003) *Biotechnology Applications of NIL, Alternative Lithography: Unleashing the Potential of the Nanoimprint Lithography*. New York, NY: Kluwer Academic/Plenum.
[8] Homola J (2008) Surface plasmon resonance sensors for detection of chemical and biological species. *Chemical Reviews* 108: 462–493.
[9] Willets KA and Van Duyne RP (2007) Localized surface plasmon resonance spectroscopy and sensing. *Annual Review of Physical Chemistry* 58: 267–297.
[10] Svedendahl M, Chen S, Dmitriev A, and Käll M (2009) Refractometric sensing using propagating versus localized surface plasmons: A direct comparison. *Nano Letters* 9: 4428–4433.
[11] Ebbesen TW, Lezec HJ, Ghaemi HF, *et al.* (1998) Extraordinary optical transmission through sub-wavelength hole arrays. *Nature* 391: 667–669.
[12] Henzie J, Lee MH, and Odom TW (2007) Multiscale patterning of plasmonic metamaterials *Nature Nanotechnology* 2: 549.
[13] Boltasseva A (2009) Plasmonic components fabrication via nanoimprint. *Journal of Optics A: Pure and Applied Optics* 11: 114001–114011.
[14] Malic L, Cui B, Tabrizian M, and Veres T (2009) Nanoimprinted plastic substrate for enhanced surface plasmon resonance imaging detection. *Optics Express* 17: 20386–20392.
[15] Hulme JP, An SSA, Goddard N, *et al.* (2009) Fabrication of a flexible multi-referenced surface plasmon sensor using room temperature nanoimprint lithography. *Current Applied Physics* 9: e185–e188.
[16] Jorgenson RC (2001) A surface plasmon resonance side active retro-reflecting sensor. *Sensors and Actuators B* 73: 236–248.
[17] Lucas BD, Kim, JS, Chin C, and Guo LJ (2008) Nanoimprint lithography based approach for the fabrication of large-area, uniformly-oriented plasmonic arrays. *Advanced Materials* 20: 1129–1134.
[18] Chen J, Shi J, Decanini D, *et al.* (2009) Gold nanohole arrays fabricated by using soft UV nanoimprint lithography. *Microelectronic Engineering* 86: 632–635.
[19] Cui B and Veres T (2007) Fabrication of metal nanoring array by nanoimprint lithography (NIL) and reactive ion etching. *Microelectronics Engineering* 84: 1544–1547.
[20] Li K, Cui B, Clime L, and Veres T (2007) Fabrication of SERS active substrates by nanoimprint lithography. In: *MRS Proceedings* 1054-FF01-03. http://www.mrs.org/s_mrs/sec_subscribe.asp?CID=11325%26DID=224868&action=detail
[21] Li K, Clime L, Cui B, and Veres T (2008) Surface enhanced Raman scattering on long-range ordered noble-metal nanocrescent arrays. *Nanotechnology* 19: 145305.
[22] Alvarez-Puebla R, Cui B, Bravo-Vasquez JP, *et al.* (2007) Nanoimprinted SERS active substrate with tunable surface plasmon resonance. *Journal of Physical Chemistry C* 111: 6720–6723.
[23] Alvarez-Puebla R, Bravo-Vasquez JP, Cui B, *et al.* (2007) SERS classification of highly related performance enhancers. *ChemMedChem* 2: 1165–1167.
[24] Li K, Clime L, Tay L, *et al.* (2008) Multiple surface plasmon resonances and near infrared field enhancement of gold nanowells. *Analytical Chemistry* 80: 4945–4950.
[25] Cui B, Clime L, Li K, and Veres T (2008) Fabrication of large area nanoprism arrays and their application for surface enhanced Raman spectroscopy. *Nanotechnology* 19: 145302.
[26] Chao CY and Guo LJ (2006) Design and optimization of microring resonators in biochemical sensing application. *Journal of Lightwave Technology* 24: 1395–1401.
[27] Fan X, White IM, Zhu H, *et al.* (2007) Overview of novel integrated optical ring resonator bio/chemical sensors. *Proceedings of SPIE* 6452: 64520M.
[28] Densmore A, Vachon M, Xu DX, *et al.* (2009) Silicon photonic wire biosensor array for multiplexed real-time and label-free molecular detection. *Optics Letters* 34: 3598.
[29] Chao CY and Guo LJ (2003) Biochemical sensors based on polymer microrings with sharp asymmetrical resonance. *Applied Physics Letters* 83: 1527.
[30] Wei D, Bailey MJ, Andrew P, and Ryhänen T (2009) Electrochemical biosensors at the nanoscale. *Lab on a Chip* 9: 2123–2131.
[31] Koehne JE, Chen H, Cassell AM, *et al.* (2004) Miniaturized multiplex label-free electronic chip for rapid nucleic acid analysis based on carbon nanotube nanoelectrode arrays. *Clinical Chemistry* 50: 1886–1893.
[32] Sandison ME and Cooper JM (2006) Nanofabrication of electrode arrays by electro-beam and nanoimprint lithographies. *Lab on a Chip* 6: 1020.
[33] Tallal J, Peyrade D, Lazzarino F, *et al.* (2005) Replication of sub-40 nm gap nanoelectrodes over an 8-in. substrate by nanoimprint lithography. *Microelectronic Engineering* 78–79: 676–681.
[34] Curreli M, Zhang R, Ishikawa FN, *et al.* (2008) Real-time, label-free detection of biological entities using nanowire-based FETs. *IEEE Transactions on Nanotechnology* 7: 651–667.
[35] Gao C, Deng SR, Wan J, *et al.* (2010) 22 nm silicon nanowire gas sensor fabricated by trilayer nanoimprint and wet etching. *Microelectronic Engineering* 87: 927–930.
[36] Ghatnekar-Nilsson S, Karlsson I, Kvennefors A, *et al.* (2009) A new multifunctional platform based on high aspect ratio interdigitated NEMS structures. *Nanotechnology* 20: 175502.
[37] Cao H, Yu Z, Wang J, *et al.* (2002) Fabrication of 10 nm enclosed nanofluidic channels. *Applied Physics Letters* 81: 174.
[38] Guo LJ, Chang X, and Chou CF (2004) Fabrication of size-controllable nanofluidic channels by nanoimprinting and its application for DNA stretching. *Nano Letters* 4: 69–73.
[39] Liang X and Chou SY (2008) Nanogap detector inside nanofluidic channel for fast real-time label-free DNA analysis. *Nano Letters* 8: 1472–1476.

[40] Bilenberg B, Hansen M, Johansen D, *et al.* (2005) Topas-based lab-on-a-chip microsystems fabricated by thermal nanoimprint lithography. *Journal of Vacuum Science and Technology B* 23: 2944–2949.
[41] Geissler M, Li K, Cui B, *et al.* (2009) Plastic substrates for surface-enhanced Raman scattering. *Journal of Physical Chemistry C* 113: 17296–17300.
[42] Britland S, Perridge C, Denyer M, *et al.* (1996) Morphogenetic guidance cues can interact synergistically and hierarchically in steering nerve cell growth. *Experimental Biology Online – EBO* 1: 2.
[43] Guillemette MD, Cui B, Roy E, *et al.* (2009) Surface topography induces 3D self-orientation of cells and extracellular matrix resulting in improved tissue function. *Integrative Biology* 1: 196–204.
[44] Matsuzaka K, Walboomers XF, Yoshinari M, *et al.* (2003) The attachment and growth behavior of osteoblask-like cells on microtextured surfaces. *Biomaterials* 24: 2711–2719.
[45] Hu W, Yim EKF, Reano RM, *et al.* (2005) Effects of nanoimprinted patterns in tissue-culture polystyrene on cell behavior. *Journal of Vacuum Science and Technology B* 23(6): 2984–2989.
[46] Johansson F, Carlberg P, Danielsen N, *et al.* (2006) Axonal outgrowth on nano-imprinted patterns. *Biomaterials* 27: 1251–1258.
[47] Heidi Au HT, Cui B, Chu ZE, *et al.* (2009) Cell culture chips for simultaneous application of topographical and electrical cues enhance phenotype of cardiomyocytes. *Lab on a Chip* 9: 564–575.
[48] Charest JL, Eliason MT, García AJ, *et al.* (2005) Polymer cell culture substrates with combined nanotopographical patterns and micropatterned chemical domains. *Journal of Vacuum Science and Technology B* 23(6): 3011–3014.
[49] Curtis ASG, Gadegaard N, Dalby MJ, *et al.* (2004) Cells react to nanoscale order and symmetry in their surroundings. *IEEE Transactions on Nanobioscience* 3: 61–65.
[50] Wilkinson CDW, Riehle M, Wood M, *et al.* (2002) The use of materials patterned on a nano- and micro-metric scale in cellular engineering. *Materials Science and Engineering C* 19: 263–269.
[51] Bogue R (2008) Nanosensors: A review of recent progress. *Sensor Review* 28: 12–17.
[52] Bogue R (2009) Nanosensors: A review of recent research. *Sensor Review* 29: 310–315.
[53] Stewart MEAnderton CR, Thompson LB, (2008) Nanostructured plasmonic sensors. *Chemical Reviews* 108: 494–521.
[54] Hutter E and Fendler JH (2004) Exploitation of localized surface plasmon resonance. *Advanced Materials* 16: 1685–1706.
[55] Sepúlveda B, Angelomé PC, Lechuga LM, and Liz-Marzán LM (2009) LSPR-based nanobiosensors. *Nano Today* 4: 244–251.
[56] Pumera M, Angelomé PC, Lechuga LM, and Liz-Marzán LM (2007) Electrochemical nanobiosensors. *Sensors and Actuators B* 123: 1195–1205.
[57] Yogeswaran U and Chen S(2008) A review on the electrochemical sensors and biosensors composed of nanowires as sensing material. *Sensors* 8: 290–313.
[58] Wei D, Bailey MJA, Andrew P, and Ryhänen T (2009) Electrochemical biosensors at the nanoscale. *Lab on a Chip.* 9: 2123–2131.
[59] Qin L, Zou S, Xue C (2006) Designing, fabricating, and imaging Raman hot spots.*Proceedings of the National Academy of Sciences* 103: 13300–13303.
[60] Jäckel F, Kinkhabwala AA, and Moerner WE (2007) Gold bowtie nanoantennas for surface-enhanced Raman scattering under controlled electrochemical potential. *Chemical Physics Letters* 446: 339–343.
[61] Su K, Durant S, Steele JM, (2006) Raman enhancement factor of a single tunable nanoplasmonic resonator. *Journal of Physical Chemistry B* 110: 3964.
[62] Wang S, Pile DF, Sun C, and Zhang X (2007) Nanopin plasmonic resonator array and its optical properties. *Nano Letters* 7: 1076.
[63] Stiles PL, Dieringer JA, Shah NC, and Van Duyne RP (2008) Surface-enhanced Raman spectroscopy. *Annual Review of Analytical Chemistry* 1: 601–626.
[64] Sun L, and Irudayaraj J (2008) Quantitative surface-enhanced Raman for gene expression estimation. *Biophysical Journal* 96: 4709–4716.
[65] Banholzer MJ, Millstone JE, Qin L, and Mirkin CA (2008) Rationally designed nanostructures for surface-enhanced Raman spectroscopy. *Chemical Society Reviews* 37: 885–897.
[66] Hering K, Cialla D, Ackermann K, (2008) SERS: A versatile tool in chemical and biochemical diagnostics. *Analytical and Bioanalytical Chemistry* 390: 113–124.
[67] Porter MD, Lipert RJ, Siperko LM, Wang G, and Narayanan R (2008) SERS as a bioassay platform: Fundamentals, design, and applications. *Chemical Society Reviews* 37: 10001–10011.
[68] Qian XM, and Nie SM (2008) Single-molecule and single-nanoparticle SERS: From fundamental mechanisms to biomedical applications. *Chemical Society Reviews* 37: 912–920.
[69] Lim C, Hong J, Chung BG, deMello AJ, and Choo J (2010) Optofluidic platforms based on surface-enhanced Raman scattering. *Analyst* 135: 837–844.
[70] Erickson D, Mandal S, Yang AHJ, and Cordovez B (2008) Nanobiosensors: Optofluidic, electrical and mechanical approaches to biomolecular detection at the nanoscale. *Microfluidics and Nanofluidics* 4: 33–52.
[71] Roy S and Gao Z (2009) Nanostructure-based electrical biosensors. *Nano Today* 4: 318–334.
[72] Perry JL and Kandlikar SG (2006) Review of fabrication of nanochannels for single phase liquid flow. *Microfluidics and Nanofluidics* 2: 185–193.
[73] Bhatia SN and Chen CS (1999) Tissue engineering at the micro-scale. *Biomedical Microdevices* 2(2): 131–144.
[74] Teixeira Al Abrams GA, Bertics PJ, Murphy CJ, and Nealey PF (2003) Epithelial contact guidance on well-defined micro- and nano-structured substrates. *Journal of Cell Science* 116: 1881–1892.
[75] Wojciak-Stothard B, Curtis A, Monaghan W, MacDonald K, and Wilkinson C (1996) Guidance and activation of murine macrophages by nanometric scale topography. *Experimental Cell Research* 223: 426–435.
[76] Rajnicek AM, Britland S, and McCaig C (1997) Contact guidance of CNS neurites on grooved quartz: Influence of groove dimensions, neuronal age and cell type. *Journal of Cell Science* 110: 2905–2913.
[77] Dalby MJ, Riehle MO, Johnstone H , Affrossman S , and Curtis ASG (2002) *In vitro* reaction of endothelial cells to polymer demixed naontopography. *Biomaterials* 23: 2945–2954.
[78] Dalby MJ, Riehle MO, Johnstone H , Affrossman S , and Curtis ASG (2004) Investigating the limits of filopodial sensing: A brief report using SEM to image the interaction between 10 nm high nano-topography and fibroblast filopodia. *Cell Biology International* 28: 229–236.
[79] Yim EKF, Reano RM, Pang SW, (2005) Nanopattern-induced changes in morphology and motility of smooth muscle cells. *Biomaterials* 26: 5405–5413.

Relevant Websites

http://www.ornl.gov – Oak Ridge National Laboratory; Biosensors and Other Medical and Environmental Probes.
http://www.sciencedirect.com – Sciverse; Biosensors and Bioelectronics.